ELSEVIER

Journal of Wind Engineering
and Industrial Aerodynamics 63 (1996) 77–93

JOURNAL OF
wind engineering
AND
industrial
aerodynamics

Application of a non-convex model of fabric deformations to sail cut analysis

O. Le Maître[a,*], S. Huberson[a,1], J.E. Souza de Cursi[b]

[a]*LaME, BP 540, 76058 Le Havre Cedex, France*
[b]*INSA de Rouen, BP 08, 76131 Mt. St. Aignan, France*

Abstract

In this paper, we present a computer model based on an elastic string network representation for sail deformation. The equilibrium equation for this model is written in the form of a minimization problem. The latter is non-convex because of the unilateral-stress behaviour of strings. The method of deconvexification has to be used in order to obtain an equivalent problem which is easier to solve. The resulting model is applied to sail cut design problems: bi- and tri-radial cut plans are compared, as well as variations of the elasticity modulus in warp and weft directions. The results are found to be very similar to what is usually observed on actual sail boats.

1. Introduction

The main property of soft sails is probably their adjustability to very different wind conditions. They are the only asymmetrical airfoil which can be used with the same efficiency for positive as well as negative angles of incidence. These properties result from the mechanical characteristics of the fabrics used in sail fabrication. Beside this, from a mechanical point of view, fabrics are anisotropic and offer poor resistance to shear. This last point is usually improved by coating sailcloth with resin filler.

As a consequence, a computer model has to include all the main aspect of actual sail behaviour in order to be useful for sail makers. The usual models are based on the elastic membrane, or shell, large deformation theories. These models take into account two of the main characteristics of sails:

- The thickness is negligible compared to the characteristic length of the sail whereas the curvature radius remains large. Thus, the motion of the sail can be described by equations written on the mean surface.

* Corresponding author.
[1] E-mail: hu@cher.univ-lehavre.fr.

PII S0165-0114(96)00070-0

• Due to their flexibility, the sail undergoes large displacements which cannot be described by means of a linear theory and the equations have to be written on the actual sail mean surface.

Such models can be found, for instance, in the pioneering works of Mutin [3], and Jackson [1]. Although all these methods are able to provide realistic results, it must be pointed out that CPU time as well as numerical difficulties introduce severe limitations when considering industrial applications: these methods are generally considered as academic.

The main feature of sail problems is that the sail can undergo large deformations without any significant internal strains. This is the result of fabric flexibility and the corresponding equilibrium shape is expected to be as close as possible to the sail maker's guess. Moreover, it is well known that sail never exactly fits that shape. This is due, for a part, to the tuning of the sail by the crew, and for another part, to the non-uniform aerodynamic load, which eventually will be supported by the sail.

The model which is proposed in this paper has been designed in order to account for these phenomena. It is based on a representation of the sail by a network of stress unilateral strings. The constitutive strings are as much as possible representative of the warp-and-weft direction. This will be particularly important in the discrete model since the mesh will have to satisfy this condition. The string model is presented in Section 3 and its extension to the string network model and the complete theory is briefly described in Section 4. Then, the decomposition of the sail into a finite-element mesh, based on the fabric panelling of actual sail is considered (Section 5). In Section 6, numerical results obtained with the present model are presented and commented on. Various cases are considered, depending on the plan cut of the sail and fabric orientation. The solutions show a realistic behaviour of the model compared to observations of real sails, and show its capability to deal with sail cut analysis.

2. Approximation of a fabric by means of a string network

Common fabrics (yarn for example) used for sails are obtained by weaving two families of strings, the weft and the warp. The resulting string network is then coated in order to improve its mechanical behaviour to bias loads (weft has usually the higher elasticity modulus direction while warp has the lower. These two moduli, as well as the coating, combine to provide the bias elasticity modulus (45°). Thus, the fabric is anisotropic and its mechanical characteristics usually provided by the factories are diagrams for loads and elongations, for different loading directions. An example of such a diagram is provided in Fig. 1.

Note that sail makers, when dealing with sail cut, usually attempt to align as much as possible the weft direction with the field of internal stresses, in order to minimize elastic deformations. The bias tensions are assumed to remain small and can be neglected. The conception basis simply relies on the analysis of strains, in the weft-and-warp directions. Thus, a string's network model is obtained by assuming that the tensions result from strains in individual strings.

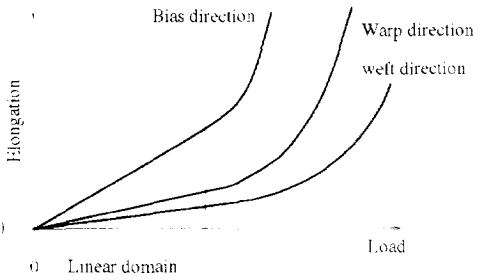

Fig. 1. Elongation versus load for weft, warp and bias loading directions.

3. The string model

A string is a one-dimensional structural object: its configuration is given by an application associating a natural curvilinear coordinate $s \in \mathscr{R}$ to a vector $\boldsymbol{X}(s) \in \mathscr{R}^3$, the position of the particle s. The deformation of the string is characterized by the unitary strains

$$\varepsilon(s) = \|\boldsymbol{X}_{,s}\| - 1, \tag{1}$$

$$\boldsymbol{X}_{,s} = \mathrm{d}\boldsymbol{X}/\mathrm{d}s. \tag{2}$$

The characteristic length of the string's section is supposed to be very small when compared to its total length. If, in addition, we limit our theory to the practical situation where the radii of curvature of the mean line remain large, flexion stresses can be neglected. Under these assumptions, an ideally flexible behaviour can be assumed: the mechanical behaviour of the string is entirely characterized by, on the one hand, its internal forces given by the field of tensions $\boldsymbol{T}(s)$ (the tension is $T(s) = \|\boldsymbol{T}(s)\|$) and, on the other hand, its modulus of elasticity $K(s)$. The local strain $\varepsilon(s)$ and the tension $\boldsymbol{T}(s)$ are connected by the relations:

$$T = K\varepsilon, \tag{3}$$

$$\boldsymbol{T} = T\frac{\boldsymbol{X}_{,s}}{\|\boldsymbol{X}_{,s}\|}. \tag{4}$$

Moreover, strings have a *stress unilateral property*: compression cannot be physically realized. Under a compressive force, the mechanical reaction includes a modification of its shape such that compression vanishes: one usually says that a string cannot transmit compressive stresses since it would immediately buckle. This property is illustrated in Fig. 2 and is later referred to as "unilateral" behaviour.

The unilateral behaviour implies that all the internal forces are traction forces:

$$T \geqslant 0 \underbrace{\Leftrightarrow}_{\text{Eq. (3)}} \varepsilon \geqslant 0 \underbrace{\Leftrightarrow}_{\text{Eq. (2)}} \|\boldsymbol{X}_{,s}\| \geqslant 1. \tag{5}$$

So, the tension T and, equivalently, the strain ε are both non-negative: the unilateral behaviour appears as a restriction to the configurations of the string. In fact, let us

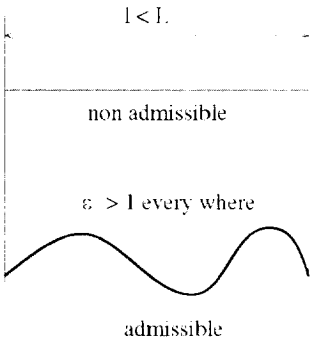

Natural length of the string is l.

Fig. 2. Illustration of the unilateral behaviour of a string.

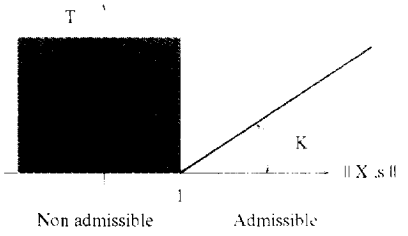

Fig. 3. Relation between tension and strain.

consider that the following usual boundary conditions are given: the position of the ends, denoted by $\boldsymbol{X}_0$ and $\boldsymbol{X}_L$. Then the set of the admissible configurations of the string reads as

$$\mathcal{V} = \{\boldsymbol{X} \mid \boldsymbol{X}(s=0) = \boldsymbol{X}_0,\ \boldsymbol{X}(s=L) = \boldsymbol{X}_L,\ \|\boldsymbol{X}_{,s}\| \geqslant 1\}. \tag{6}$$

Due to Eq. (5), the set of admissible displacements is non-convex: this property follows from the relation between tension and strain illustrated in Fig. 3.

4. The string network model

4.1. Definition of the internal stresses

We consider a piece of fabric described by a set of natural curvilinear coordinates, the first one aligned with the weft direction is denoted a_{f}, and the second with the warp: a_{w}. The shape is completely defined by the knowledge of a mapping which associates $a = (a_{\mathrm{f}}, a_{\mathrm{w}}) \in \Omega$ to a position $\boldsymbol{X}(a) \in \mathscr{R}^3$ (see Fig. 4).

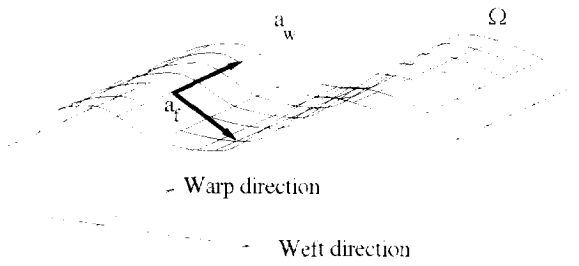

Fig. 4. Approximation of fabric by string network.

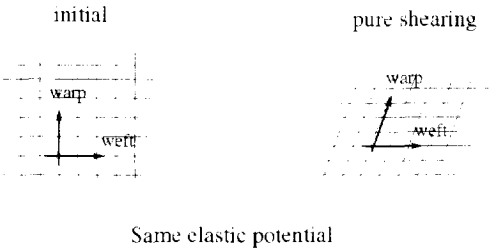

Fig. 5. Shear stresses are neglected.

The extension of the string's model to the string's network one is straightforward: we introduce elongations and tensions relative to weft-and-warp directions by

$$\varepsilon_i = \|\boldsymbol{X}_{,i}\| - 1, \tag{7}$$

$$T_i = K_i \varepsilon_i, \tag{8}$$

$$T_i \geqslant 0, \tag{9}$$

$$\boldsymbol{T}_i = T_i \frac{\boldsymbol{X}_{,i}}{\|\boldsymbol{X}_{,i}\|}, \tag{10}$$

where $i = \mathrm{f}, \mathrm{w}$. The elastic potential is given by

$$W(\boldsymbol{X}) = \int\int_{\Omega} (K_{\mathrm{f}} \varepsilon_{\mathrm{f}}^{\,2} + K_{\mathrm{w}} \varepsilon_{\mathrm{w}}^{\,2})\, \mathrm{d}a. \tag{11}$$

As previously remarked, this expression does not involve energy due to bending and bias strains, which are neglected in this model (see Fig. 5).

4.2. *Equilibrium of a network of strings*

Let us consider that the fabric is submitted to a given external field of forces with surface density $\boldsymbol{f}(a) \in \mathscr{R}^3$ (this is the situation when iterative calculations of aerodynamic forces/sail's equilibrium are considered, for instance). Then the equilibrium of

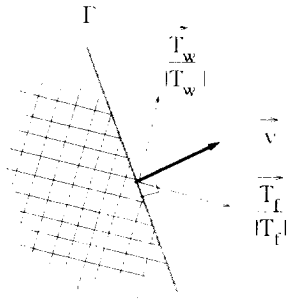

Fig. 6. Definition of the normal to the boundary.

the network reads as

$$\boldsymbol{T}_{f,i} + \boldsymbol{T}_{w,i} + \boldsymbol{f} = \boldsymbol{0} \quad \forall a \in \Omega. \tag{12}$$

Let us denote by $\partial\Omega$ the boundary of Ω. Let Γ_0 be the part of $\partial\Omega$ which is fixed and Γ the edges allowed to move. Thus, the boundary conditions are:

$$\boldsymbol{X}(a) = \boldsymbol{X}_0(a), \quad \forall a \in \Gamma_0, \tag{13}$$

$$v_f \boldsymbol{T}_f + v_w \boldsymbol{T}_w = \boldsymbol{h}, \quad \forall a \in \Gamma, \tag{14}$$

where $v_i = \boldsymbol{v} \cdot \boldsymbol{T}_i / T_i$ and $\boldsymbol{v}$ is the normal unit to Γ and tangent to the sail's mean surface (see Fig. 6) and $\boldsymbol{h}$ is an external force applied on Γ.

We consider

$$V = \{\boldsymbol{y} : \Omega \Rightarrow \mathscr{R}^3\}, \tag{15}$$

$$V_0 = \{\boldsymbol{v} \in V \mid \boldsymbol{v} = \boldsymbol{0} \text{ on } \Gamma_0\}, \tag{16}$$

where V is the set of displacements $\boldsymbol{y}$ defined on Ω, and V_0 is its reduction to the displacements $\boldsymbol{v}$, null on Γ_0. The set of admissible configurations is

$$\mathscr{V} = \{\boldsymbol{X} \mid \boldsymbol{X} = \boldsymbol{X}_0 + V, \ \|\boldsymbol{X}_{,i}\| \geqslant 1 \ \forall a \in \Omega, \ i = \mathrm{f}, \mathrm{w}\}. \tag{17}$$

Analogously to the one-dimensional model, $\mathscr{V}$ is a non-convex set.

4.3. Functional Resolution

Let us introduce:

$$U(\boldsymbol{T}, [\boldsymbol{u}_1, \boldsymbol{u}_2]) = \int\int_\Omega (\boldsymbol{T}_f \cdot \boldsymbol{u}_1 + \boldsymbol{T}_w \cdot \boldsymbol{u}_2)\, \mathrm{d}a, \tag{18}$$

$$H([\boldsymbol{c}, \boldsymbol{f}], \boldsymbol{u}) = \int_\Gamma \boldsymbol{c} \cdot \boldsymbol{u}\, \mathrm{d}\Gamma + \int\int_\Omega \boldsymbol{f} \cdot \boldsymbol{u}\, \mathrm{d}a.$$

The configuration of equilibrium can be characterized by the following variational formulation associated to Eq. (12), analogous to the principle of virtual work.

Problem 1. $\boldsymbol{X} \in \mathcal{V}$, $U(\boldsymbol{T}(\boldsymbol{X}), [\boldsymbol{v}_{,\mathrm{f}}, \boldsymbol{v}_{,\mathrm{w}}]) + H([\boldsymbol{F}, \boldsymbol{h}], \boldsymbol{v}) = 0, \ \forall \boldsymbol{v}/\boldsymbol{v} \in V_0.$ (19)

Eq. (19) means that, for $\boldsymbol{X}$ solution and any admissible displacement field $\boldsymbol{v}$: the virtual work of internal stresses (U) is equal to the virtual work of external loads (H). Problem 1 is a non-convex variational problem which can be functionally studied by the method of convexification, which provides an associated convex problem for the determination of the field of tensions $\boldsymbol{T} = \boldsymbol{T}_{\mathrm{f}} + \boldsymbol{T}_{\mathrm{w}}$, which is uniquely determined. This second problem is obtained by replacing ε_i by ε_i^* in (5) and (6) with ε_i^* defined as

$$\varepsilon_i^* = \|\boldsymbol{X}_{,i}\| - 1, \quad \|\boldsymbol{X}_{,i}\| \geqslant 1,$$

$$\varepsilon_i^* = 0, \quad \|\boldsymbol{X}_{,i}\| < 1.$$

We denote by U^* the form analogous to U obtained by considering ε^* instead of ε in the definition of $\boldsymbol{T}$. Then the convexified problem reads as

Problem 2. $\boldsymbol{X} \in \boldsymbol{X}_0 + V$, $U^*(\boldsymbol{T}(\boldsymbol{X}), [\boldsymbol{v}_{,\mathrm{f}}, \boldsymbol{v}_{,\mathrm{w}}]) + H([\boldsymbol{F}, \boldsymbol{h}], \boldsymbol{v}) = 0, \ \forall \boldsymbol{v}/\boldsymbol{v} \in V_0.$ (20)

As remarked, the resolution of Problem 2 gives the field of tension solution of Problem 1. It can be shown (see Ref. [2]) that if ε_{f} and ε_{w} are strictly positive everywhere, then the two problems are equivalent and uniqueness of the solution holds. If zero-tension parts exist anywhere, the problems are equivalent only for the tensions, which are uniquely determined: different configurations lead to the same field of tensions and multiple configurations of equilibrium do exist. We assume thereafter that the loads applied to a sail are such that $\|\boldsymbol{X}_{,i}\| \geqslant 1$ everywhere so that Problems 1 and 2 are equivalent: they lead to the same solution for the deformations as well as for the tensions.

5. Application to sails

5.1. Sail panelling

The starting point of a sail concept is the definition of the shape that the sailmaker wants to obtain. This shape is generally a surface of $\mathscr{R}^3$. This target is then approximated by panelling the surface into a set of small fabric pieces which are then patched together. The resulting structure is thus the juxtaposition of different panels of fabric on which we can use the string network model. The complete configuration is then defined as an atlas of maps, for every panel (see Fig. 7).

We have to deal with a variational problem which is the sum of elementary Problems 2 for every panel constituting the sail. The continuity of $\boldsymbol{X}$ and $\boldsymbol{v}$ over the whole sail

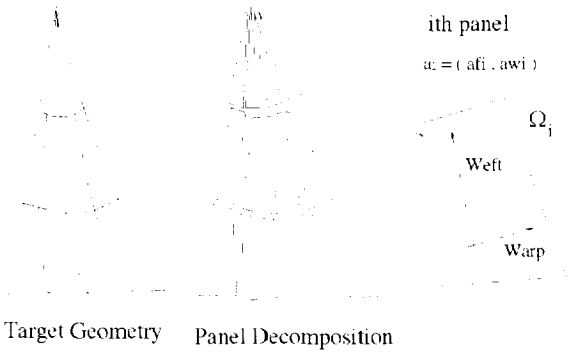

Fig. 7. Panel decomposition and map definition.

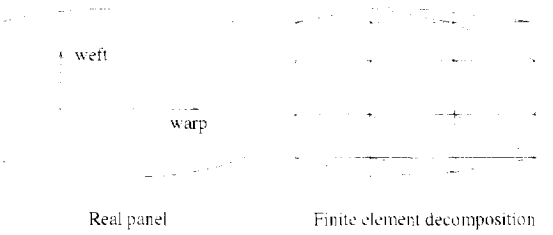

Fig. 8. Decomposition of the panel by triangular finite elements.

provides an additional constraint. The boundary condition in (14) states that the tension has to be continuous ($\boldsymbol{T}_i \cdot \boldsymbol{v}_i = \boldsymbol{T}_j \cdot \boldsymbol{v}_j$ with i and j two neighbouring panels) as well.

5.2. *Finite-element approximation*

On every panel, Problem 2 is approached using a standard finite-element method [4]. Each panel is divided into triangular elements, two sides of which are aligned with the local weft-and-warp directions as illustrated in Fig. 8.

Denoting by $\boldsymbol{\Xi}$ the vector of the discrete *nddl* degrees of freedom of the structure, these finite-element approximations lead to a system of *nddl* non-linear equations having the form

$$\mathscr{L}(\boldsymbol{\Xi}) = \boldsymbol{0}. \tag{21}$$

An iterative procedure is used to solve this set of equations: from a given configuration $\boldsymbol{\Xi}^0$ the solution is found out by the series

$$\mathscr{L}(\boldsymbol{\Xi}^k) = \boldsymbol{R}^k, \tag{22}$$

$$\boldsymbol{\Xi}^{k+1} = \boldsymbol{\Xi}^k - \omega \boldsymbol{R}^k, \tag{23}$$

where ω is an under-relaxation coefficient. The computations are stopped when the iteration number k is large enough or $\|\boldsymbol{R}^k\| < \delta R$ with δR a given precision, small enough to ensure a correct convergence.

6. Numerical results

6.1. Definition of a reference case

We now present numerical results. In order to have an easy analysis of the results, all the computations have been performed with the same initial shape. It has been defined by an analytical mapping: $z = s(x, y)$. As a consequence, initial shapes are expected to be independent of the mesh used.

For the same reason, the external loads have been defined as an analytical function $\boldsymbol{df} = \boldsymbol{d}f(x, y)z$ from the initial shape and then assumed to remain constant during the deformation process. The sail is fixed by the luff, the head and the tack in the plane $z = 0$, it is 3.8 m high with a 2 m long foot. The initial shape is plotted in Fig. 9, and the magnitude of the external loads in Fig. 10.

For the time being, the fabric has been assumed to have a constant modulus of elasticity for warp-and-weft, equal to $K = 1 \times 10^3$. The surface of the sail must then be approximated by the finite-elements constitutive of the mesh. As mentioned in the introduction, this is a particular problem since the anisotropic behaviour of sailcloth has to be correctly approximated by the mesh through the string network scheme. In other words, not only the numerical results but the exact solution will be strongly related to the grid definition. This grid has been built according to the following principle: first of all, the sail is divided into blocks which are provided by the sail cut and defined by the sailmaker. Then, for each block, two families of curves have been defined and provide a grid with square cells. These families are aligned as closely as possible with the warp-and-weft directions in order to obtain a string network which is a good

Fig. 9. Initial shape (natural configuration). Grey level correspond to different values of $z = s(x, y)$.

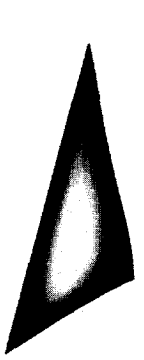

Fig. 10. Magnitude of external loads. Grey level correspond to different values of external loads $df(x, y)$.

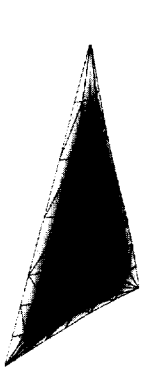

Fig. 11. Equilibrium configuration for 82 elements – grey scale for the value of $z(x, y)$ of equilibrium shape and mesh.

approximation of the warp-and-weft network of the actual sail. A triangular mesh is then obtained by dividing each cell into two triangles.

6.2. *Convergence of the solution with mesh refinement*

We consider a tri-radial cut for the sail, the weft directions are basically rays issuing from the sail corners and constitute angular sectors dividing the sail into three blocks (see mesh in Fig. 13). Computations were performed for different refinements of the mesh using, respectively, 82, 170 and 348 elements for the same tri-radial cut. The corresponding equilibrium configurations are plotted in Figs. 11–13.

From these numerical tests, we can point out that the model does not require too many elements to provide a good estimation of the maximum value of the hollow. In fact, there is no significant variation of the computed hollow magnitude as well as for

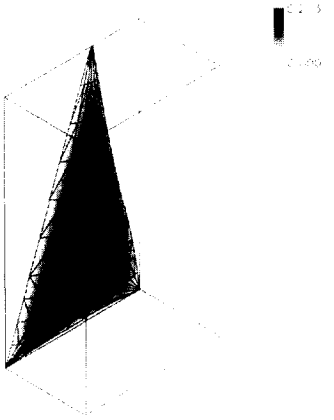

Fig. 12. Equilibrium configuration for 170 elements – grey scale for the value of $z(x, y)$ of equilibrium shape and mesh.

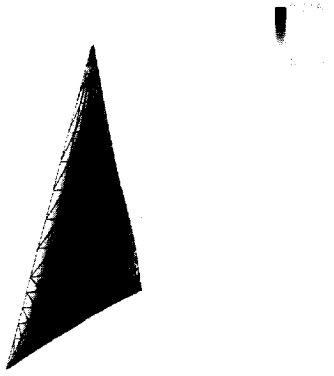

Fig. 13. Equilibrium configuration for 348 elements – grey scale for the value of $z(x, y)$ of equilibrium shape and mesh.

its distribution on the surface when using a finer mesh with 348 elements, instead of 170. Thus, the 170 elements mesh is used hereafter. Moreover, we can observe that the displacements at the centre of the sail from the initial shape are important, even if the strains remain small. This fact is due to displacements of the free edges that lead to a finite displacement at the centre. This illustrates the capability of the model to deal naturally with large displacement problems.

6.3. *The effect of fabric orientation*

The effect of the fabric anisotropy has also been investigated. We consider two different values for the modulus of elasticity for the warp (K_w) and weft (K_f) directions.

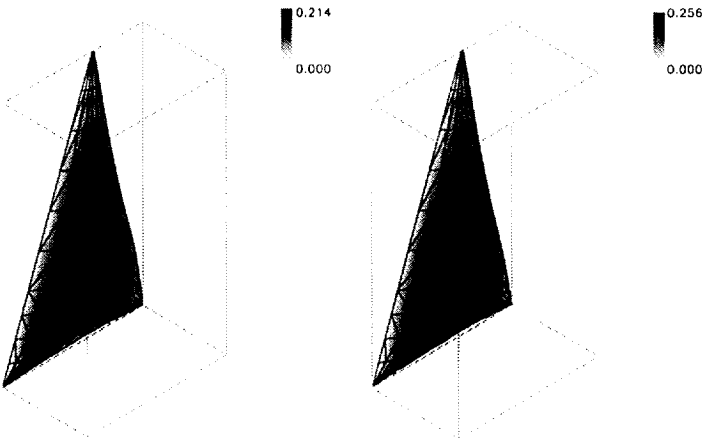

Fig. 14. Equilibrium configurations for oriented fabric case 1 (left) and case 2 (right) – grey scale for the values of $z(x, y)$ of equilibrium geometries and meshes.

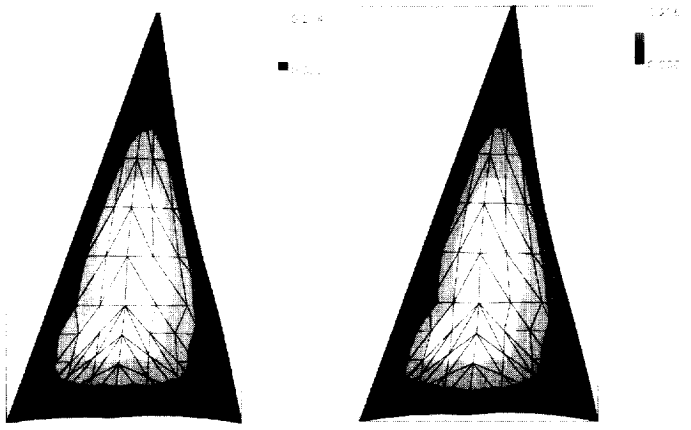

Fig. 15. Projection of hollow in the plane $z = 0$ for case 1 (left) and case 2 (right), grey levels correspond to different values of hollow.

We set K_f at 1×10^3 and K_w at 2×10^2 and the computation is performed for two cases:

Case 1: The fabric is well orientated so that the weft directions are aligned with the tri-radial panelling. It is expected that the weft is roughly aligned with the strain direction almost everywhere in that case.

Case 2: The warp-and-weft direction are swapped, or more simply, K_w and K_f values are exchanged.

The results are presented in Figs. 14 and 15. They show that for case 1, the weft is actually aligned with the internal tensions and small variations of the warp mod-

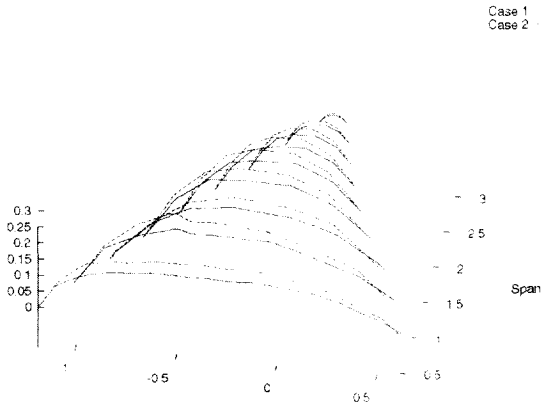

Fig. 16. Comparison of equilibrium profiles for cases 1 and 2.

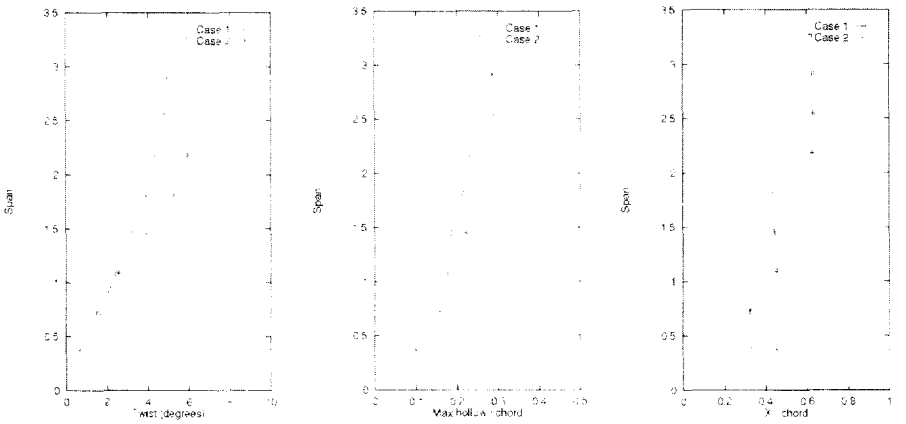

Fig. 17. Comparison of twist angles (left), maximum of hollow (centre) and its chord location (right) for different spanwise sections for cases 1 and 2. Hollow values and their locations are scaled with the local chord length.

ulus of elasticity do not induce large changes in the equilibrium shape. On the contrary, if the weft-and-warp modulus of elasticty are exchanged, noticeable variations of the solution have been obtained which is exactly what could have been expected (see Figs. 16 and 17). In Fig. 17 the discontinuity in the location of the maximum of the hollow is due to the finite-element discretization since the maximum is necessarily located on one side of an element and then the location has to switch from one side to the other. This numerical example illustrates the capability of the model to deal with oriented fabric when weft-and-warp directions have different modulus K. Moreover, we know that the equilibrium shape for a given field of external loads depends partly on the mechanical characteristic of the fabric used, and partly on the panelling of the surface. This point is investigated in the next section.

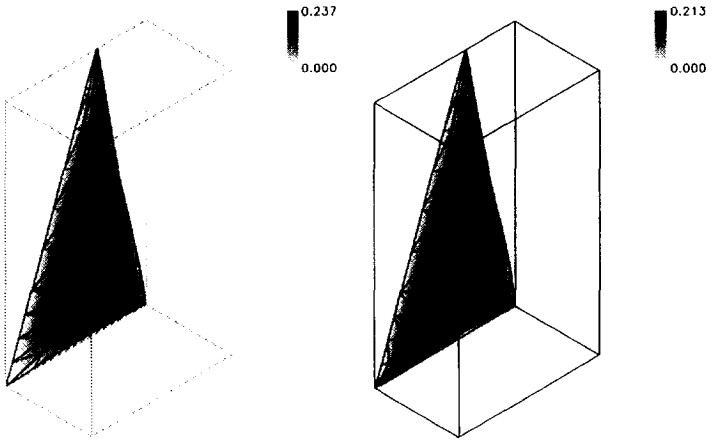

Fig. 18. Equilibrium configurations for bi-radial (left) and tri-radial (right) sail cut - grey scales for different values of $z(x, y)$ of equilibrium geometries and meshes.

6.4. *Influence of sail cut on deformations*

In fact, the panelling of the surface is the key point of the sail design procedure since it will determine the orientation of the fabric with respect to the sail plan. Different technological choices in panelling lead to different deformations under the same loading conditions. This point induces many difficulties in sail design and require adaptable prediction tools. The string network model can deal with these kind of problems and we present some results obtained for two different cut plans of the same surface. The initial geometries are still the same as the previous one, and we consider two different panellings of the surface. The first one is a decomposition of the surface by a bi-radial cut, while the second is the tri-radial mesh which has been used in the previous section. Both are discretized using 170 elements. The corresponding equilibrium shapes are plotted in Figs. 18 and 19.

As expected, we can note that the two solutions are different. The maximum value of the hollow is greater for the bi-radial cut (see Figs. 19 and 20). The distribution of the hollow on the surface is different too; for the tri-radial panelling the hollow is more uniform along the span. For the bi-radial cut, a larger hollow in the upper part has been obtained. Once again, this is due to a larger deformation of the free leech. As a result, at a given station, not only will the camber of the sail profile be affected, but the twist angle as well.

6.5. *Influence of load magnitude*

In this section, we investigate the effect of an increased wind speed. The bi- and tri-radial meshes are used to perform the same computations with an external load multiplied by four. This is roughly equivalent to doubling the wind speed. In Fig. 21,

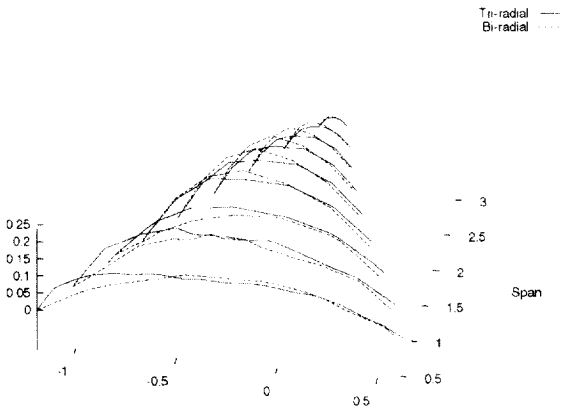

Fig. 19. Comparison of equilibrium profiles for bi- and tri-radial cuts.

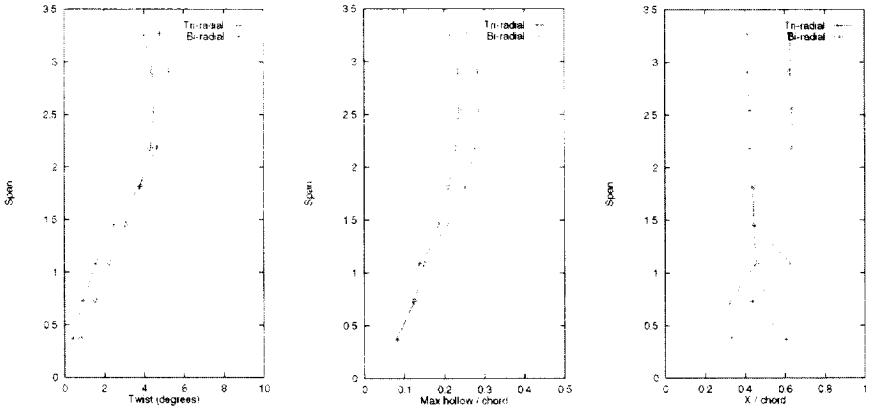

Fig. 20. Comparison of twist angles (left), maximum of hollow (centre) and its chord location (right) for different spanwise sections for tri- and bi-radial cuts. Hollow values and their locations are scaled with the local chord length.

the projection of the hollow value on the plane $z = 0$ is plotted for bi- and tri-radial cuts and both magnitudes of external loads. We can observe the displacement of the hollow for the two cuts. For both cases, the hollow moves back in the direction of the trailing edge and becomes deeper. Moreover, it is clear that the hollow distribution along the span is uniform for the two loads and tri-radial cut, compared to the bi-radial sail which permits a displacement of the hollow towards the head when the loads are increased.

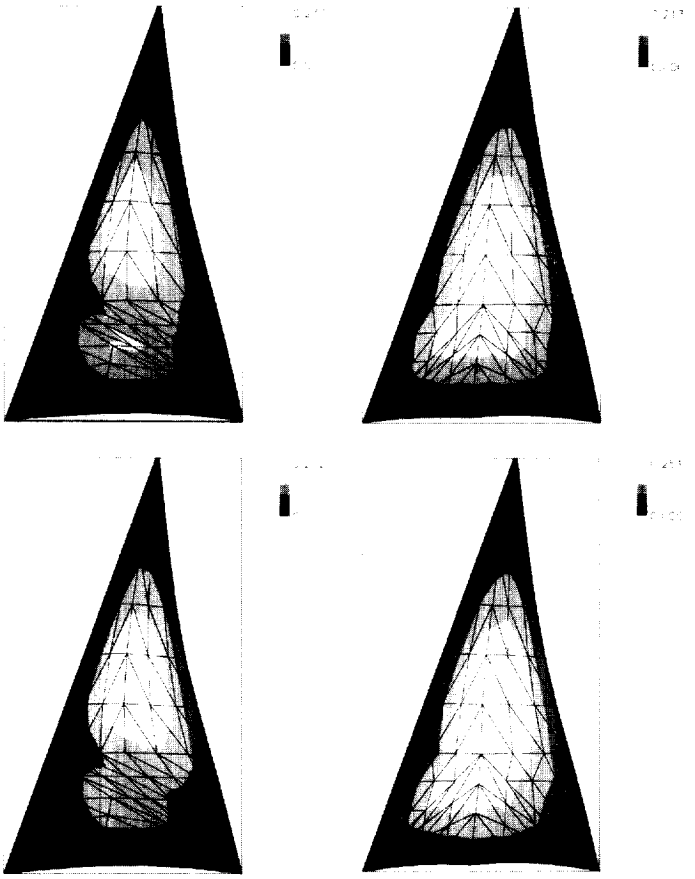

Fig. 21. Projection in plane $z = 0$ of equilibrium configurations for bi-radial (left), tri-radial (right) sail cut and initial (top) or four-times external loads (bottom) — grey levels correspond to different values of hollow.

7. Conclusions

An elastic string network model of sails has been proposed. It has been used to simulate some real life problems of sail design. The ability of the model to reproduce what can be expected from our knowledge of reality is very satisfactory. The tendency is good for any of the studied cases. However, one must keep in mind that all the problems considered in this paper are "virtual" in the sense that the numerical results have not been compared to real sail data. To undertake this task would require three parts at least:

- to be able to reproduce numerically actual sailing conditions,
- to derive a coupled algorithm in order to introduce in the present model the aerodynamic loads resulting from the previous point.
- to have data obtained for real sails in real sailing conditions.

It can be expected that solving the first two points will require a large amount of hard work. This will not be enough for the last point which needs also a special financial effort. We hope that the present development of research in this domain will soon enable us to apply our computer model to real sails, otherwise any improvement will soon become meaningless.

Acknowledgements

We would like to thank Région Haute Normandie, who supported this project.

References

[1] P.S. Jackson and G.W. Christie, Numerical analysis of three-dimensional elastic membrane wings, AIAA J. 25 (1986) 676–682.
[2] J.E. Souza de Cursi, Un probleme issu de l'étude des fils sans raideur soumis au frottement sec, Ann. de la Faculté des Sci. de Toulouse XI(2) (1990) 137–186.
[3] F. Mutin, Modélisation de membrane. application à l'analyse mécanique des voiles de bateau, Ph.D. Dissertation, Université de Nice Sophia Antipolis (1989).
[4] O.C. Zienkiewicz, The Finite Element Method in Engineering Sciences (McGraw-Hill, New York, 1977).